Progress In Electromagnetics Research M, Vol. 110, 185–195, 2022

Sea-Surface Slow Small Target Detection Based on Polarimetric Multi-Domain Feature Fusion

Chun-Ling Xue[1, *], Fei Cao[1], Qing Sun[2], Jian-Feng Xu[1], and Xiao-Wei Feng[1]

Abstract—A target detection method based on polarimetric multi-domain feature fusion is proposed in this paper to improve the detection performance of slow small targets on the sea. Firstly, a complex symmetric matrix was established based on the Pauli scattering vector. On the basis of an analysis on the matrix, the Takagi decomposition method was adopted to extract the normalized polarimetric maximum eigenvalue to characterize the echo signal. Secondly, a real symmetric Hurst exponent matrix was constructed by processing the echo signal of the polarimetric radar, and the normalized polarimetric Hurst exponent was extracted by the eigenvalue decomposition method. Thirdly, the normalized polarimetric Doppler peak height was extracted through the Doppler peak height algorithm. Finally, by fusing multi-domain features, a false alarm controllable detector was constructed through the convex hull algorithm. The results of experimental analysis on the measured datasets indicate that when the parameters are the same, compared with the traditional detection methods based on polarimetric features, the proposed method presents better robustness in the case of short observation time and low signal to clutter rate.

1. INTRODUCTION

When a radar detects targets on the sea, the receiver synchronously receives the scattering echo from the sea surface, namely the sea clutter. It is prone to overshadow the echo signal of small targets and undermine the detection performance of radar [1]. In terms of the sea clutter under the illumination of a high-resolution radar with a low gazing angle, its amplitude distribution obtained by statistical methods is non-Gaussian, non-stationary, nonlinear, and with a long trail [2–4]. Thus, it is difficult for modelling. Moreover, in frequency domain analysis, the Doppler frequency of slow small targets usually shifts within a wide frequency band of sea clutter, which increases the difficulty of distinguishing targets from sea clutter [5]. In recent years, the radar cross-section (RCS) of the target radar has become smaller with the development of stealth technology, which makes it more difficult for a radar to detect low, slow, and small targets. Therefore, how to optimize the performance of radar detection of slow small targets on the sea has become an important research direction in the development of radar detection technologies in recent years.

In view of the above characteristics of sea clutter, some scholars have explored target detection methods based on features. Literature [6] pointed out that the sea clutter approached fractal at a certain scale interval based on the research on the fractal theory of sea clutter, but the performance of target detection decreased when the clutter was beyond the interval. In [7], three features of time and frequency domains were used for the sea surface target detection, and a new idea of feature fusion was proposed. In [8], the multi-domain features of time, frequency, and fractal dimensions were used for information fusion, which improved the detection performance of targets on the sea in a single polarimetric channel.

Received 17 March 2022, Accepted 19 May 2022, Scheduled 1 June 2022
* Corresponding author: Chun-Ling Xue (Chling_xue@163.com).
[1] High-Tech Institute of Xian, Xi'an, Shaanxi 710025, China. [2] School of Mathematics and Information Science, Baoji University of Arts and Sciences, Baoji, Shaanxi 721013, China.

According to the research on scattering characteristics of sea clutter in [9, Chapter 2], the echo signal from the polarimetric radar contained rich target information. With the development of ubiquitous radar technologies, based on the polarimetric radar, some scholars have carried out research on the detection of targets on the sea at low gazing angles [1, 10–12]. In [10], the distance between entropy and anisotropy (DBEA) was obtained by the polarimetric eigenvalue decomposition method, and the empirical threshold was combined for target detection. In [1], the coherent decomposition method of the polarimetric covariance matrix was adopted to obtain three polarimetric scattering components. In [11], the five-dimensional features were extracted from two polarimetric decomposition angles for target detection. However, the method can generate inaccurate decomposition results and have poor anti-interference ability. Also, in [12], on the basis of the classic tri-feature method, the performance of detecting targets on the sea at short observation time was improved by fusing polarimetric time-domain and frequency-domain features, while the in-depth exploration has not been carried out on the features of other transform domains.

Based on the polarimetric radar, this paper proposes a target detection method based on polarimetric multi-domain feature fusion. Firstly, a complex symmetric matrix was constructed by the Pauli scattering vector, and the Takagi decomposition method was adopted to extract the time-domain normalized polarimetric maximum eigenvalue (NPME). Secondly, the normalized polarimetric Hurst exponent (NPHE) and normalized polarimetric Doppler peak height (NPDH) were extracted from the fractal and frequency domains, respectively. Finally, a false-alarm controllable convex hull detector was constructed by fusing multi-domain features to achieve the detection of slow small targets on the sea.

2. OBJECT DETECTION MODEL AND MEASURED DATASETS

2.1. Object Detection Model

The detection of targets on the sea by polarimetric radar was generally deemed as a binary hypothesis testing problem [12], and the detection model is

$$\begin{cases} H_0: \begin{cases} \mathbf{r}_J(n) = \mathbf{c}_J(n) \\ \mathbf{r}_{J,p}(n) = \mathbf{c}_{J,p}(n) \end{cases} \\ H_1: \begin{cases} \mathbf{r}_J(n) = \mathbf{s}_J(n) + \mathbf{c}_J(n) \\ \mathbf{r}_{J,p}(n) = \mathbf{c}_{J,p}(n) \end{cases} \end{cases} \\ n = 1, 2, \cdots, N;\ J = HH, VV, HV, VH;\ p = 1, 2, \cdots, P \tag{1}$$

where the null hypothesis H_0 represents that there is no target in a bin to be tested. The alternative hypothesis H_1 represents that there are targets in the bin. $\mathbf{r}(n)$, $\mathbf{s}(n)$, and $\mathbf{c}(n)$ represent radar echo, target echo, and sea clutter echo, respectively. n, p, and J represent the pulse sequence, reference bin, and polarimetric channel, respectively. N and P represent the pulse length and the number of reference bins, respectively.

2.2. Measured Dataset

The verification experiment in this paper adopts the shared measured datasets of the IPIX radar [13]. The datasets were collected in Dartmouth in 1993 by experimental staff at McMaster University. Specifically, the foam ball is 1 m in diameter covered with metal strips as a target. The radar carrier frequency is 9.34 GHz, and the sampling frequency is 1 kHz. Each dataset contains 14 bins, and the sampling pulse of each bin is 131072. Table 1 presents other related parameters. The selected measured datasets in Table 1 cover a variety of sea states, polarimetric channels, and signal to clutter rate (SCR). SCR is calculated as follows [7]:

$$\mathrm{SCR} = 10\log_{10}\left(\frac{P_T - P_C}{P_C}\right) \tag{2}$$

where P_T represents the average power of the echo signals of the target bins. P_C represents the average power of echo signals of clutter bins.

Table 1. Description of IPIX radar datasets.

File	Primary Target	Second Target	SCR/dB	Wave/m
#26	7	6, 8	5.5	1.1
#54	8	7, 9, 10	14.8	0.7
#280	8	7, 9, 10	5.8	1.6
#310	7	6, 8, 9	2.7	0.9
#320	7	6, 8, 9	11.5	0.9

3. TARGET DETECTION METHOD BASED ON POLARIMETRIC MULTI-DOMAIN FEATURE FUSION

Based on the analysis on polarimetric radar echo signals, their multi-domain features are extracted from the time domain, fractal, and frequency domain, respectively. A false alarm controllable detector is constructed by fusing multi-domain features and adopting the convex hull algorithm. In the following feature analysis, the observation time is all selected as 512 ms, and the adjacent data segments are processed by sliding 64 points each time.

3.1. Polarimetric Multi-Domain Features

3.1.1. Normalized Polarimetric Maximum Eigenvalue

Sinclair scattering matrix is the basic recording unit of polarimetric radar, and its elements describe the scattering characteristics of a target under different polarimetric channels. Based on the Pauli matrix decomposition and reciprocity theorem (i.e., $S_{HV} = S_{VH}$) [11], the polarimetric scattering matrix can be vectorized as a Pauli scattering vector $\mathbf{k}_P$, which is expressed as follows:

$$\mathbf{k}_P = \frac{1}{\sqrt{2}}\left[\begin{array}{ccc} S_{HH} + S_{VV} & S_{HH} - S_{VV} & 2S_{HV} \end{array}\right]^T \tag{3}$$

where S_J $(J = HH, VV, HV, VH)$ is the element of the Sinclair scattering matrix. The first capital letter of the subscript indicates the received polarimetric mode; the second capital letter of the subscript indicates the transmitted polarimetric mode; and $[\cdot]^T$ denotes the transpose. The first element of Pauli scattering vector denotes the single scattering from a plane surface, and the second and third elements denote the diplane scattering from corners with a relative orientation of 45°, respectively.

The extraction method of the normalized polarimetric maximum eigenvalue is as follows. The convolution of the Pauli scattering vector is carried out to obtain the complex symmetric matrix of the single-view echo, and then to obtain the multi-view expectation matrix at the observation time. Afterwards, the Takagi decomposition method is adopted to solve the non-negative real number diagonal matrix of the expected matrix and to extract the largest eigenvalue. Finally, the maximum eigenvalue of the bins to be tested is compared with the sum of the maximum eigenvalues of each bin extracted at the corresponding observation time. The quotient is the NPME feature at the time domain.

The specific steps of extracting the feature are as follows:

a) Find the expectation of the complex symmetric matrix. Based on the Pauli scattering vector $\mathbf{k}_P$, the complex symmetric matrix of the single-view echo is constructed by means of the convolution operation. The expectation of the echo complex symmetric matrix founded at the observation time is marked as $\mathbf{M}$, and the equation is

$$\mathbf{M} = \left\langle \mathbf{k}_P \otimes \mathbf{k}_P^T \right\rangle = \left[\begin{array}{ccc} T_{11} & T_{12} & T_{13} \\ T_{21} & T_{22} & T_{23} \\ T_{31} & T_{32} & T_{33} \end{array}\right] \tag{4}$$

where $\langle\cdot\rangle$, $\otimes$, and superscript T denote expectation, Kronecker product, and transpose, respectively. The matrix $\mathbf{M}$ obtained by convolution and expectation processing can suppress clutter and noise

interference, and improve the SCR. The elements of $\mathbf{M}$ are as follows:

$$\begin{cases} T_{11} = \dfrac{1}{2}\left\langle (S_{HH} + S_{VV})^2 \right\rangle \\ T_{12} = T_{21} = \dfrac{1}{2}\left\langle (S_{HH})^2 - (S_{VV})^2 \right\rangle \\ T_{13} = T_{31} = \langle (S_{HH} + S_{VV})\, S_{HV} \rangle \\ T_{22} = \dfrac{1}{2}\left\langle (S_{HH} - S_{VV})^2 \right\rangle \\ T_{23} = T_{32} = \langle (S_{HH} - S_{VV})\, S_{HV} \rangle \\ T_{33} = 2\left\langle (S_{HV})^2 \right\rangle \end{cases} \tag{5}$$

b) Choose the largest eigenvalue of $\mathbf{M}$. The Takagi decomposition method was adopted to obtain the diagonal matrix $\mathbf{\Lambda}$ composed of non-negative real numbers, then to extract the largest eigenvalue [14]. The decomposition equation $\mathbf{M}$ is

$$\mathbf{M} = \mathbf{U}\Lambda\mathbf{U}^T \tag{6}$$

where $\mathbf{U}$ is a unitary matrix, and the diagonal element $\mathbf{\Lambda}$ is set as $\lambda_1 \geq \lambda_2 \geq \lambda_3 \geq 0$. The maximum eigenvalue λ_1 represents the main scattering component in the radar irradiation area after smoothing.

c) Extract NPME. To reduce the influence of the echo fluctuation at different observation times and scale differences in the fusion of features in different transform domains, a comparison between the maximum eigenvalue of the bin to be tested and the sum of the maximum eigenvalues of bins at the corresponding observation time is conducted in the paper. The quotient is NPME and marked as ξ_1. The feature is computed by

$$\xi_1 = \frac{\lambda_1}{\sum_{p=1}^{P} \lambda_{1,p}} \tag{7}$$

where $\lambda_{1,p}$ denotes the largest eigenvalue of the pth bin. For inhomogeneous sea clutter along range bins, the denominator of Eq. (7) can fit the variation of sea clutter level with range.

Figure 1 shows the NPME histograms of sea clutter and target of the #54 and #310 datasets. The results in Figure 1(a) indicate that under high SCR conditions, the NPME of sea clutter is mainly concentrated in the interval [0, 0.1]. The NPME of the target is mainly concentrated in the interval [0.3, 0.5]. Obviously, the target and sea clutter were of high separability. The results in Figure 1(b) indicate that the distribution of sea clutter and target becomes wider with the decrease of SCR. The NPME of the sea clutter is mainly concentrated in the interval [0, 0.1], while that of the target is relatively scattered, approaching uniform distribution. Both are partially intersected. The figure illustrates that the separability of NPME decreases with the reduction of SCR, so other features need to be fused to improve the separability of target and sea clutter.

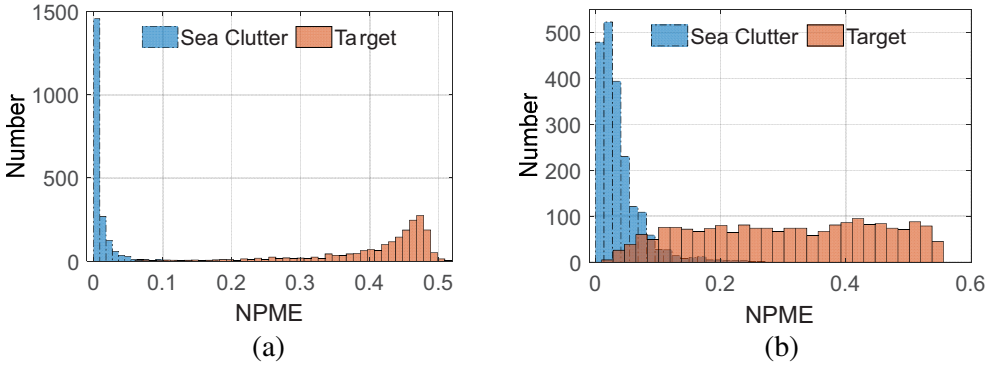

Figure 1. NPME Histograms of sea clutter and target of the (a) #54 and (b) #310 datasets.

3.1.2. Normalized Polarimetric Hurst Exponent

Fractal characterizes the roughness of the system and shows the difference in terms of self-similarity between natural objects and man-made objects. When a radar irradiates the sea surface, there is also a fractal difference between the naturally formed sea clutter and the echo signals of man-made targets. In a single polarimetric channel, the fractal characteristics fluctuate greatly. Hence, in this section, the multi-dimensional fractal information contained in the polarimetric radar echo signal is utilized to construct a polarimetric Hurst exponent matrix. Then, the eigenvalue decomposition method is adopted to obtain the NPHE of the matrix.

The specific steps of extracting the feature are as follows:

a) Construct a random walk process of the radar echo. Firstly, to suppress the influence of Gaussian white noise, the radar echo signal is preprocessed by zero mean. Assuming that the radar echo signal in any polarimetric channel is $\mathbf{r}_J(n)$, the zero-mean value sequence $\mathbf{y}_J(n)$ is obtained by removing the mean value. The equation is as follows:

$$\begin{cases} \mathbf{y}_J(n) = \mathbf{r}_J(n) - \mu_J \\ \mu_J = \dfrac{1}{N}\displaystyle\sum_{n=1}^{N} \mathbf{r}_J(n) \end{cases} \tag{8}$$

Secondly, the random walk process $\mathbf{z}_J(n)$ of the radar echo signal is obtained on the basis of the new sequence $\mathbf{y}_J(n)$. The equation is as follows:

$$\mathbf{z}_J(n) = \sum_{i=1}^{n} \mathbf{y}_J(i) \tag{9}$$

b) Choose the maximum eigenvalue of the polarimetric Hurst exponent matrix. The amplitude sequence of sea clutter shows multifractal characteristics in a certain scale range. More specifically, this is a power-law relation, i.e., Hurst index [15]. Since the existence of a target affects the change of Hurst index of sea clutter, the Hurst index feature can be used for target detection. The power law relation is

$$\begin{aligned} &\mathbf{F}_J(m) = \left\langle \left|\mathbf{z}(k+m) - \mathbf{z}(k)\right|^2 \right\rangle^{1/2} \sim m^{H_J} \\ &k = 1, 2, \cdots, N-m; \;\; J = HH, VV, HV, VH \end{aligned} \tag{10}$$

where m and H_J denote the scale and Hurst exponent in the J polarimetric channel, respectively. $\mathbf{F}_J(m)$ denotes the cumulates corresponding to m scale.

The target to be tested is a man-made object, and its energy is mainly concentrated on the maximum eigenvalue of the matrix. In comparison, the sea clutter is regarded as a natural object, and its energy is relatively dispersed. Therefore, the maximum eigenvalue of the matrix can be selected as the feature to improve the separability of target and sea clutter.

Based on the reciprocity theorem, the Hurst exponents in HH, VV, and HV polarimetric channels are selected to generate a Hurst exponent vector. Then, the polarimetric Hurst exponent matrix $\mathbf{Z}$ is constructed through convolution. $\mathbf{Z}$ is a real symmetric matrix, and the maximum eigenvalue of the matrix can be obtained by the eigenvalue decomposition method. The equations are as follows:

$$\begin{cases} \mathbf{Z} = \mathbf{W} \otimes \mathbf{W}^T = \mathbf{Q}\mathbf{V}\mathbf{Q}^T \\ \mathbf{W} = \begin{bmatrix} H_{HH} & H_{VV} & H_{HV} \end{bmatrix}^T \\ \varepsilon = \max(\mathbf{V}) \end{cases} \tag{11}$$

where $\mathbf{W}$ and $\mathbf{Z}$ are the vector and matrix of Hurst exponent, respectively. ε is the largest eigenvalue of $\mathbf{Z}$. $\mathbf{Q}$ is an orthogonal matrix composed of eigenvectors of $\mathbf{Z}$. $\mathbf{V}$ is a real diagonal matrix. The first equation in (11) is the eigenvalue decomposition of the Hurst matrix; the second equation is the vector of Hurst exponent; and the third equation is to extract the maximum value of real diagonal matrix.

c) Extract NPHE. To reduce the influence of echo fluctuation at different observation times and scale differences in the fusion of features in different transform domains, the maximum eigenvalue ε of

the bin to be tested was compared with the sum of maximum eigenvalues of bins at the corresponding observation time to obtain the NPHE, which was marked as ξ_2. The feature is computed by

$$\xi_2 = \frac{\varepsilon}{\sum_{p=1}^{P} \varepsilon_p} \tag{12}$$

where ε_p denotes the largest eigenvalue of the pth bin extracted by the Hurst index method.

Figure 2 shows the NPHE histograms of sea clutter and target of the #54 and #310 datasets. Obviously, the sea clutter and target bins have similar distribution under the two kinds of SCR. The NPHE of the sea clutter is mainly concentrated in the interval [0, 0.1], and the NPHE of the target bins is mainly concentrated in the interval [0.05, 0.4]. They have a small overlap between 0.05 and 0.15. In addition, it can be seen from Figure 2(b) that the feature proposed in this section still has separability under low SCR conditions, and it presents a different distribution from that in Figure 1, indicating that this feature is highly complementary with NPME.

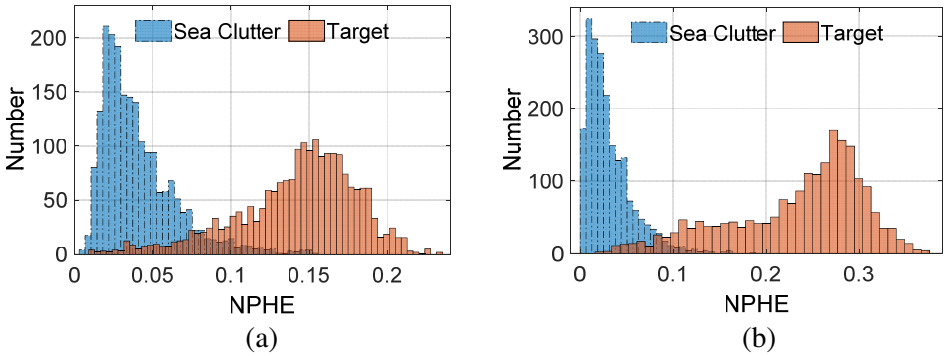

Figure 2. NPHE histograms of sea clutter and target of the (a) #54 and (b) #310 datasets.

3.1.3. Normalized Polarimetric Doppler Peak Height

According to the definition of Doppler peak height (DPH), DPH reflects the proportion of the main energy in the frequency domain [12]. In terms of the polarimetric radar, the previously selected eigenvalues are optimized to extract the NPDH in the frequency domain.

The specific steps of extracting the feature are as follows:

a) Find the average DPH of the polarimetric channel. Firstly, the DPH_J in the four polarimetric channels was calculated according to [12]. Then, its arithmetic mean value is calculated, marked as $\overline{\mathrm{DPH}}$. The equation is as follows:

$$\overline{\mathrm{DPH}} = \frac{1}{4}\left(\mathrm{DPH}_{HH} + \mathrm{DPH}_{VV} + \mathrm{DPH}_{HV} + \mathrm{DPH}_{VH}\right) \tag{13}$$

b) Extract NPDH. To reduce the influence of echo fluctuation at different observation times and scale differences in the fusion of features in different transform domains, the average DPH of the bin to be tested obtained in Eq. (13) is compared with the sum of the average DPH of bins at the corresponding observation time. The quotient is NPME and marked as ξ_3. The feature is calculated by

$$\xi_3 = \frac{\overline{\mathrm{DPH}}}{\sum_{p=1}^{P} \overline{\mathrm{DPH}}_p} \tag{14}$$

where $\overline{\mathrm{DPH}}_p$ denotes the average DPH of the pth bin.

Figure 3 shows the NPDH histograms of sea clutter and target of the #54 and #310 datasets. This indicates that the NPDH histograms of the sea clutter bins in the two datasets have a similar

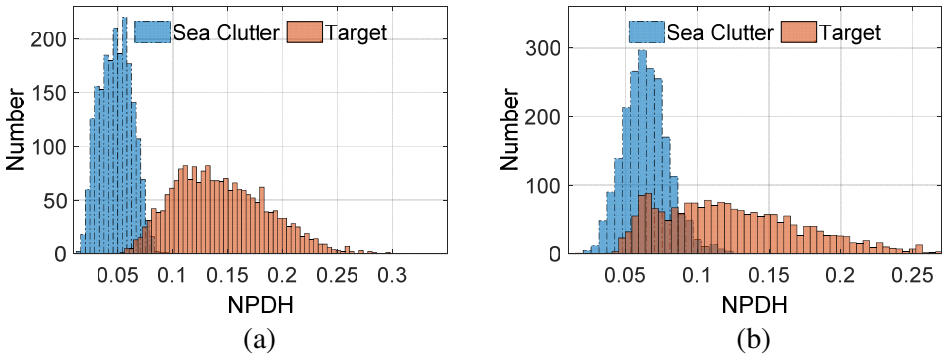

Figure 3. NPDH histograms of sea clutter and target of the (a) #54 and (b) #310 datasets.

distribution, and the NPDH mainly concentrate in the interval [0, 0.1]. In addition, the NPDH distribution center of the target bins approaches that of the sea clutter bins with the decrease of SCR. Its feature is mainly distributed in the interval [0.05, 0.25], showing a different distribution from NPME and NPHE. This indicates that the features of the three transform domains are characterized by high complementarity.

4. OBJECT DETECTION METHOD

During the detection of unknown targets on the sea, it is easier to obtain the sea clutter data than target echo signals. Thus, the targets are usually detected as the anomaly of sea clutter. Based on the convex hull algorithm's characteristics such as controllable false alarms and good visual effect in anomaly detection, a target detection method of the paper was constructed by combining full polarization multi-domain feature fusion and the false alarm controllable convex hull algorithm [1]. Among them, the optimal decision region's equation for solving the false alarm controllable convex hull algorithm is

$$\begin{cases} \Omega^c = \arg\min\limits_{\Omega} \{\text{Volume}(\Omega)\} \\ \text{s.t.} \quad \#\{i : \boldsymbol{\xi}^c \in \Omega\} = I \times (1 - P_f) \end{cases} \tag{15}$$

where Ω^c represents the optimal decision region of the training samples. Ω represents the feature space of the training samples. $\#\{A\}$ represents the number of the A. $\boldsymbol{\xi}^c$ represents the polarimetric multi-domain feature vector of the training sample. I represents the number of sea clutter training samples. P_f represents the set false alarm probability.

When the polarimetric multi-domain feature vector $\boldsymbol{\xi}^t$ of bins to be tested is in Ω^c, it is judged as H_0; otherwise, it is H_1. The basic process of the target detection method is shown in Figure 4. The

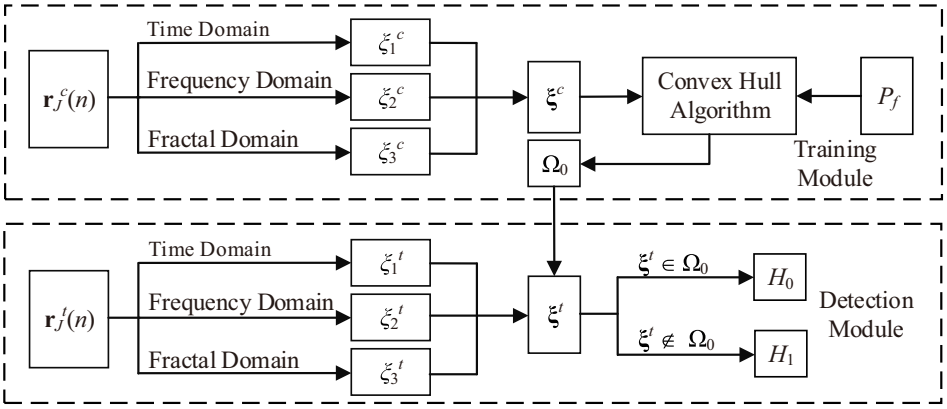

Figure 4. Flow chart of target detection based on polarimetric multi-domain feature fusion.

superscripts c and t in the figure represent the training set and the test set, respectively. The process mainly includes a training module and a detection module.

Figure 5 shows the feature space distribution of target and sea clutter bins of #54 and #310 datasets obtained by the method in this paper. In the figure, the red '$*$' represents the target, and the blue 'o' represents the sea clutter. The blue part surrounded by the polyhedron is a decision region with a false alarm probability of 10^{-3}. It is obvious that the feature space determined by the multi-domain feature vectors in this paper shows higher separability under the two kinds of SCR.

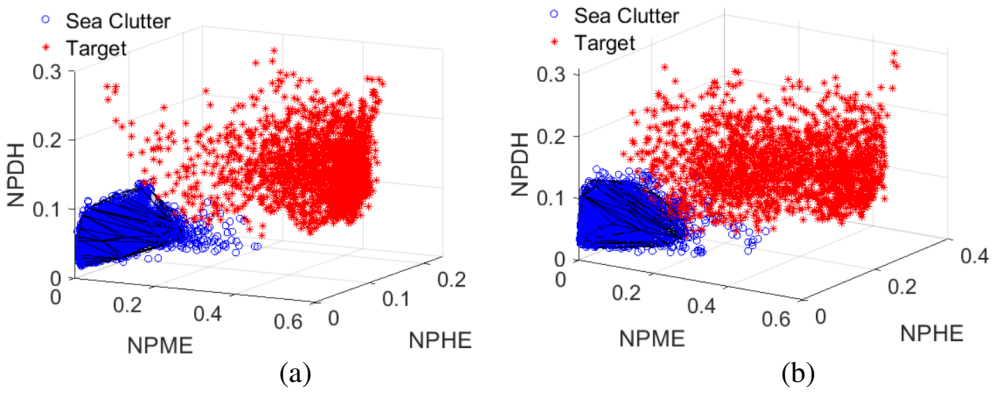

Figure 5. Multi-domain feature spaces and convex-hull decision regions of the (a) #54 and (b) #310 datasets.

5. EXPERIMENTS AND ANALYSIS

5.1. Detection Performance of the Method at Different Observation Times

In this section, the proposed method is used to calculate the detection probability (P_d) of the dataset in Table 1 at the observation time of n (ranged from 7 to 12). For other parameters, the false alarm probability (P_f) is set as 10^{-3}. Adjacent data segments are processed by sliding 64 points each time, and the obtained sample size of each dataset is more than 20000, which meets the test conditions of the convex hull algorithm.

Figures 6(a)–(e) are detection probability curves obtained by this method at different observation times, and Figure 6(f) is a curve of average detection probability. The black solid line in the figure represents a detection probability curve obtained by using a Fast Fourier transform (FFT) with a fixed frequency range of 1024 Hz during the NPDH feature extraction. The blue dotted line represents the detection probability curve obtained by using FFT, and its frequency range is determined by the observation time. The comparison among Figure 6 indicates that in #280 and #320, the black solid line shows that there is local fluctuation at the observation time of 256 ms. Because the frequency range of FFT is fixed during the extraction of NPDH features, when the observation time is less than 1024 ms, the FFT decentralizes the energy of clutter in radar echo signals. This affects the detection performance of the proposed method and results in the fluctuation of detection probability at the observed time series of some datasets. The blue dotted line is the detection probability curve obtained in NPDH feature with variable frequency range, showing that the detection probability of each dataset is consistent with the overall change trend of Figure 6(f) with the increase of observation time. However, the detection probability is lower than that of this method when the observation time is less than 512 ms. It can also be seen from Figure 6 that with the increase of observation time, the detection performance of the proposed method presents an overall upward trend, and the detection performance stays well.

5.2. Comparison of Detection Performance of Different Methods

The detection performance of the proposed method and the existing 4 polarimetric feature detection methods will be compared in this section [1, 10–12]. For convenience, the method in [10] is referred

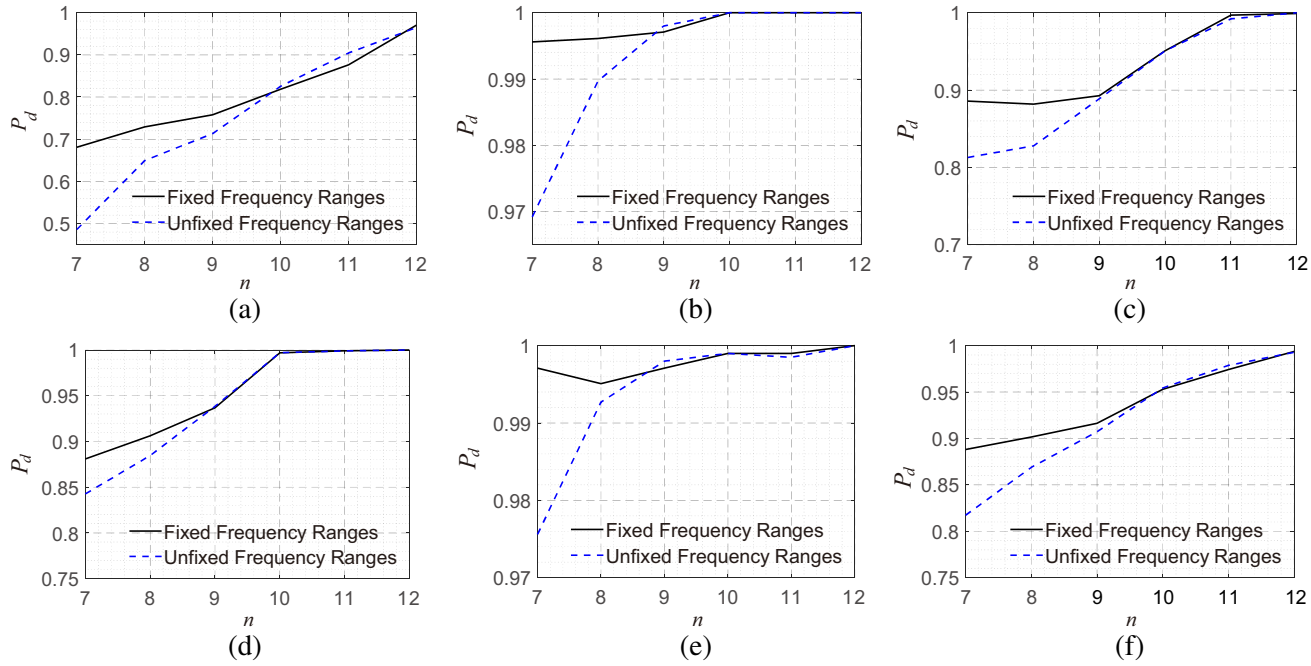

Figure 6. Detection probability of different datasets at different observation times. (a) #26, (b) #54, (c) #280, (d) #310, (e) #320, (f) mean value.

to as the distance between entropy and anisotropy (DBEA) methods. The one [12] is referred to as the tri-feature method in four polarization channels (Tri-FPC). The one in [1] is referred to as the tri-polarization-feature method (3D-PFM). The one in [11] is referred to as the combined characteristics of polarization method (CCPM).

Figure 7(a) shows the detection probabilities of the 5 methods in different datasets when the false alarm probability is 10^{-3}. Figure 7(b) shows the curve of the dataset's average ROC obtained by the 5 methods. In terms of parameter selection, the observation time is 512 ms, and the adjacent data segments are processed by sliding 64 points each time.

It can be seen from Figure 7(a) that the detection performance of the traditional detection method is greatly affected by sea states and SCR. The proposed method and Tri-FPC method have better anti-interference ability and mediate the problem of instability of polarimetric decomposition. The reason is that they fuse multi-domain features, complement each other from different transform domains and improve the target detection performance. It is worth noting that the detection performance of the proposed method is better than that of the Tri-FPC method in low SCR and high sea states, but this

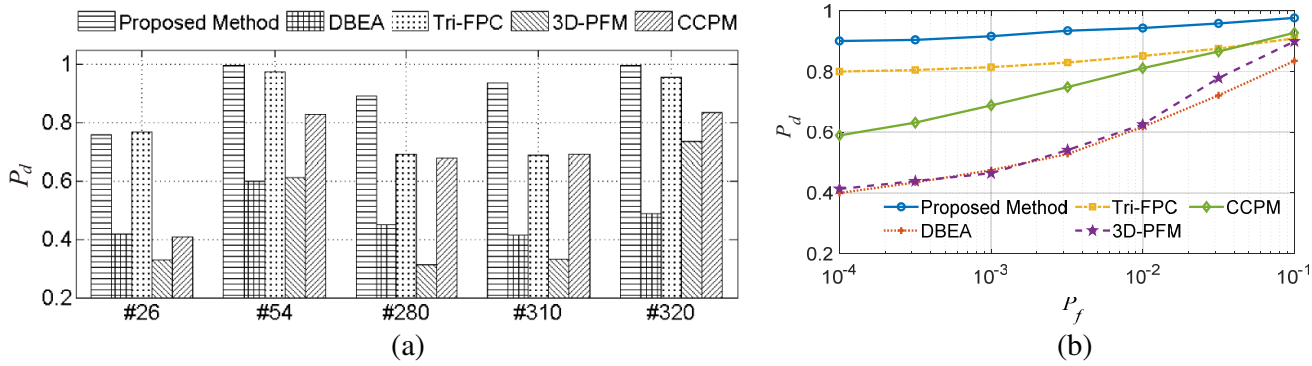

Figure 7. Detection performance of five methods. (a) Detection performance in different datasets. (b) ROC curves.

advantage decreases with the rise of sea states. Figure 7(b) compares the average detection probability of the 5 detection methods with the change of false alarm probability, illustrating that these methods have large differences when the false alarm probability is low. The sequence of their detection probability is: the proposed method > Tri-FPC method > CCPM method > 3D-PFM method > DBEA method. However, the differences gradually decrease with the increase of false alarm probability. This is because the improvement effect of multi-domain feature fusion reaches a bottleneck with the increase of false alarm probability. Furthermore, the performance of these detection methods fluctuates to a certain extent due to the influence of complex sea conditions. However, the proposed method in this paper shows better robustness, with an average detection probability greater than 90%, followed by the Tri-FPC method, whose average detection probability is greater than 80%. The other detection methods have relatively low detection performance.

6. CONCLUSION

In this paper, aiming at the difficulty of detecting slow small targets in complex sea conditions, a better distinguishable area between sea clutter and targets is obtained by fusing the multi-domain features based on the feature extraction of polarimetric radar echo signals. The comparative experimental analyses indicate that the proposed method has better robustness than other traditional methods when the SCR is low, and the observation time is less than 512 ms. What needs to be pointed out is that the features of different transform domains extracted in this paper have different distributions. Thus, how to use this distribution characteristic for target detection is also the next research direction.

ACKNOWLEDGMENT

This work has been supported by the National Natural Science Foundation of China (61903375) and by Shaanxi Provincial Natural Science Foundation (2018JQ1046).

REFERENCES

1. Xu, S., J. Zhang, J. Pu, and P. Shui, "Sea-surface floating small target detection based on polarization features," *IEEE Geoscience and Remote Sensing Letters*, Vol. 15, No. 10, 1505–1509, October 2018.
2. Weinberg, G. V. and C. Tran, "Burr distribution for X-band maritime surveillance radar clutter," *Progress In Electromagnetics Research B*, Vol. 81, 183–201, 2018.
3. Park, J.-H., D.-H. Kim, D.-H. Kim, and S. Kim, "Variation of the shape parameter of K-distribution for sea clutter with the spatial correlation of sea surface," *Progress In Electromagnetics Research Letters*, Vol. 92, 25–30, 2020.
4. Yang, M., G. Zhang, C. Guo, and M. Sun, "A coarse-to-fine approach for ship detection in SAR image based on CFAR algorithm," *Progress In Electromagnetics Research M*, Vol. 35, 105–111, 2014.
5. Li, Q., H. Zhang, and R. Lai, "Research on analysis of high-order fractal characteristics of aircraft echoes and classification of targets in low-resolution radars," *Progress In Electromagnetics Research M*, Vol. 75, 61–68, 2018.
6. Liu, N., J. Guan, J. Song, G. Wang, and Y. He, "Application of target detection based on fractal theories," *Modern Radar*, Vol. 34, No. 2, 12–18, February 2012.
7. Shui, P., D. Li, and S. Xu, "Tri-feature based detection of floating small targets in sea clutter," *IEEE Transactions on Aerospace and Electronic Systems*, Vol. 50, No. 2, 1416–1430, April 2014.
8. Xue, C., F. Cao, Q. Sun, J. Qin, and X. Feng, "Sea-surface weak target detection based on multi-feature information fusion," *Systems Engineering and Electronics*, 2022.
9. Keith, W., T. Robert, and W. Simon, *Sea Clutter: Scattering, the K Distribution and Radar Performance*, Chapter 2, Publishing House of Electronic Industry, Beijing, China, 2016.

10. Wu, P., J. Wang, and W. Wang, "Small target detection in sea clutter based on polarization characteristics decomposition," *Journal of Electronics & Information Technology*, Vol. 33, No. 4, 816–822, April 2011.
11. Chen, S., H. Gao, and F. Luo, "Target detection in sea clutter based on combined characteristics of polarization," *Journal of Radars*, Vol. 9, No. 4, 664–673, August 2020.
12. Xu, S. and J. Pu, "Floating small targets detection in sea clutter based on four-polarization-channels fusion," *Journal of Signal Processing*, Vol. 33, No. 3, 324–329, March 2017.
13. Haykin, S., "The McMaster IPIX radar sea clutter database," http://soma.ece.mcmaster.ca/ipix, 2001.
14. Yan, H. and J. Zhou, "Factorizations of complex symmetric matrices and complex skew-symmetric matrices," *Journal of Hohai University: Natural Sciences*, Vol. 36, No. 2, 283–285, March 2008.
15. Guo, Z. and P. Shui, "Anomaly based sea-surface small target detection using K-nearest neighbor classification," *IEEE Transactions on Aerospace and Electronic Systems*, Vol. 56, No. 6, 4947–4964, August 2020.